Surfactant-Free Synthesis of Bi_2Te_3−Te Micro−Nano Heterostructure with Enhanced Thermoelectric Figure of Merit

Yichi Zhang,[†] Heng Wang,[‡] Stephan Kräemer,[§] Yifeng Shi,[†,⊥] Fan Zhang,[†] Matt Snedaker,[†] Kunlun Ding,[†] Martin Moskovits,[†] G. Jeffrey Snyder,[‡] and Galen D. Stucky[†,§,*]

[†]Department of Chemistry and Biochemistry, University of California, Santa Barbara, California 93106-9510, United States, [‡]Materials Science, California Institute of Technology, 1200 East California Boulevard, Pasadena, California 91106, United States, and [§]Materials Department, University of California, Santa Barbara, California 93106-5050, United States [⊥]Present address: College of Materials, Chemistry and Chemical Engineering, Hangzhou Normal University, Hangzhou, P. R. China 310036.

ABSTRACT An ideal thermoelectric material would be a semiconductor with high electrical conductivity and relatively low thermal conductivity: an "electron crystal, phonon glass". Introducing nanoscale heterostructures into the bulk TE matrix is one way of achieving this intuitively anomalous electron/phonon transport behavior. The heterostructured interfaces are expected to play a significant role in phonon scattering to reduce thermal conductivity and in the energy-dependent scattering of electrical carriers to improve the Seebeck coefficient. A nanoparticle building block assembly approach is plausible to fabricate three-dimensional heterostructured materials on a bulk commercial scale. However, a key problem in applying this strategy is the possible negative impact on TE performance of organic residue from the nanoparticle capping ligands. Herein, we report a wet chemical, surfactant-free, low-temperature, and easily up-scalable strategy for the synthesis of nanoscale heterophase Bi_2Te_3−Te *via* a galvanic replacement reaction. The micro−nano heterostructured material is fabricated bottom-up, by mixing the heterophase with commercial Bi_2Te_3. This unique structure shows an enhanced zT value of ~0.4 at room temperature. This heterostructure has one of the highest figures of merit among bismuth telluride systems yet achieved by a wet chemical bottom-up assembly. In addition, it shows a 40% enhancement of the figure of merit over our lab-made material without nanoscale heterostructures. This enhancement is mainly due to the decrease in the thermal conductivity while maintaining the power factor. Overall, this cost-efficient and room-temperature synthesis methodology provides the potential for further improvement and large-scale thermoelectric applications.

KEYWORDS: bismuth telluride · thermoelectric material · galvanic replacement · heterostructure

Thermoelectric (TE) power generation devices play an important role in more fully utilizing abundant solar, geothermal, power plant, and automobile-derived heat *via* a noise-free and low-maintenance conversion process. Efficient use of the waste heat requires an inexpensive and scalable TE material with a high energy conversion performance. The thermoelectric figure of merit (zT), which is defined as $zT = S^2\sigma T/\kappa$, is used to evaluate the performance of TE materials at a temperature T, where S is the Seebeck coefficient, σ the electrical conductivity, and κ the thermal conductivity. A good TE material has high electrical conductivity and relatively low thermal conductivity: an "electron crystal, phonon glass" (ECPG) material.[1−12] Introducing nanoscale heterostructures into a bulk TE matrix is one way of achieving this intuitively anomalous electron/phonon transport behavior.[1,4,6,7,9,13−15] For example, Kim *et al.* grew ErAs/$In_xGa_{1-x}As$ as a heterostructured thin film by using molecular beam expitaxy (MBE).[6]

Herein, we report a simple and scalable synthesis strategy (Figure1) for producing a bulk-scale micro−nano heterostructured TE material by simply mixing the as-prepared heterophase nanoparticles (NPs) into a matrix of commercially available (microscale) powders. The key component, a nanoscaled heterophase, is normally produced by one of two routes: by reducing the grain size of a bulk material (the top-down strategy) or by growing NPs from atomic-scale assembly (the bottom-up strategy).

The top-down strategy requires high temperatures and high energy to mill melted ingots. In contrast, bottom-up assembly uses NPs as building blocks to fabricate three-dimensional heterostructured materials. The latter is a potentially more easily scalable and low-cost process. Additionally, the bottom-up approach is especially suitable for the preparation of nonstoichiometric heterophases due to the ease of controlling composition through atomic assembly. Dirmyer *et al.* recently reported the solution synthesis of bismuth telluride NPs, which

* Address correspondence to stucky@chem.ucsb.edu.

Received for review January 25, 2011 and accepted March 8, 2011.

Published online March 21, 2011
10.1021/nn2002294

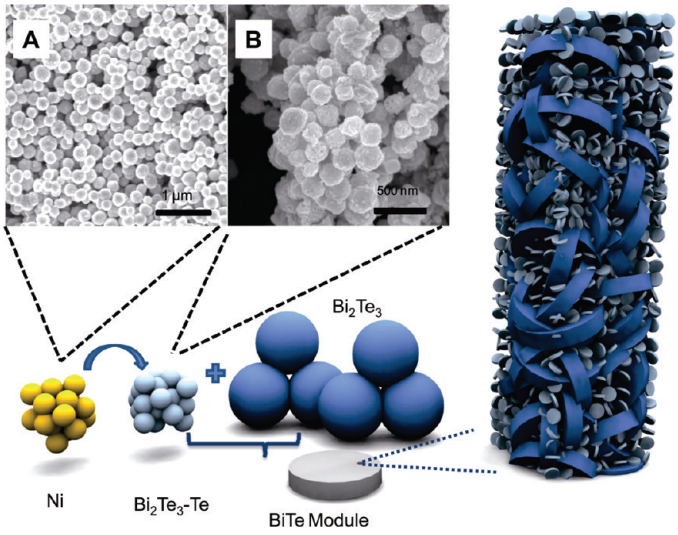

Figure 1. Synthesis procedure for micro−nano heterostructured thermoelectric material. (A) Ni nanosphere; (B) replaced nonstoichiometric bismuth telluride.

led to a number of reports on solution-grown TE NPs, especially bismuth telluride and antimony-doped bismuth telluride.[16−21] Although successful control of size and morphology was achieved, the solution-grown TE particles do not show a significant improvement in TE performance. The highest *zT* of solution-grown bismuth telluride (n-type) so far reported is 0.2 at room temperature, substantially lower than that observed for melt-grown materials (n-type 0.6).[17,18] One reason for this lower efficiency is that the NP capping ligands used during synthesis are extremely hard to remove and their thermal degradation residue can reduce the TE performance after annealing.[16] In order to solve this problem, Kovalenko *et al.* developed a ligand exchange route for removing organic capping surfactants, thereby obtaining an enhanced *zT* of 0.7 for p-type antimony-doped bismuth telluride thin films.[22] However, the exchange process for these antimony-doped materials requires hydrazine, which is toxic and reactive with oxygen, restricting the synthesis to anaerobic environments with concomitant scale-up challenges.

Instead of using an organic surfactant to control the particle growth, a surfactant-free synthesis route using a hard template to confine the particle size would be a desirable alternative and a low-cost TE synthesis. Galvanic replacement synthesis is one such facile and scalable synthesis route for preparing nanosized materials using preformed particles as both the template and reducing agent.[23−25] Recently, Myung and coworkers and Moon *et al.* demonstrated this strategy for making metal chalcogenide nanowires and nanotubes.[26−28] However, so far as we know, the preparation of bismuth telluride NPs in large quantities using galvanic replacement has not yet been reported.

In this paper, we report a novel, surfactant-free synthesis strategy based on galvanic replacement to prepare Bi_2Te_3−Te as heterophase NPs. Bismuth telluride modules embedded with nanoscale heterostructure are produced by simply mixing the nanoscale heterophase NPs into a matrix of commercially available (microscale) powders. There are several advantages to this synthesis route. It is a low-temperature process, easily scaled up. Additionally, the nonstoichiometry of the bismuth telluride nanospheres heterophase, which is expected to play a significant role in enhancing the electrical conductivity and the Seebeck coefficient, can be controlled. Finally, and importantly, the entire fabrication procedure is surfactant-free. Without the negative effects of capping ligands, the as-prepared bismuth telluride heterostructure shows a *zT* of ∼0.4, substantially higher than what was previously reported for solution-grown n-type bismuth telluride (∼0.2).[17]

RESULTS AND DISCUSSION

Figure 1 summarizes the synthesis strategy. The key step is the preparation of the Bi_2Te_3−Te nano-heterophase particles, synthesized by galvanic replacement using Ni NPs as both template and reducing agent. Ni nanospheres (Figure 1A inset) were used because the reduction potential of Ni^{2+}/Ni^0 is sufficient to reduce Bi^{3+} and $HTeO_2^+$ to form Bi_2Te_3.[27,29] The reaction (eq 1) is thermodynamically favored with an electrochemical potential of +0.803 V for $HTeO_2^+$ and H^+ concentrations of ∼0.01 and ∼0.1 M, respectively. Also, Ni makes good ohmic contact with bismuth telluride and is generally considered to be compatible to the bismuth telluride system.[30] Finally, the spherical Ni NPs result in spherical Bi_2Te_3−Te NPs that are easily packed together to produce a condensed ingot by hot-pressing.

$$2Bi^{3+}(aq) + 3HTeO_2^+(aq) + 9Ni^0(s) + 9H^+(aq) \rightarrow Bi_2Te_3(s) + 9Ni^{2+}(aq) + 6H_2O(aq) \quad (1)$$

The preformed Ni nanospheres are added to an acidic nitric solution containing Bi^{3+} and $HTeO_2^+$ ions.

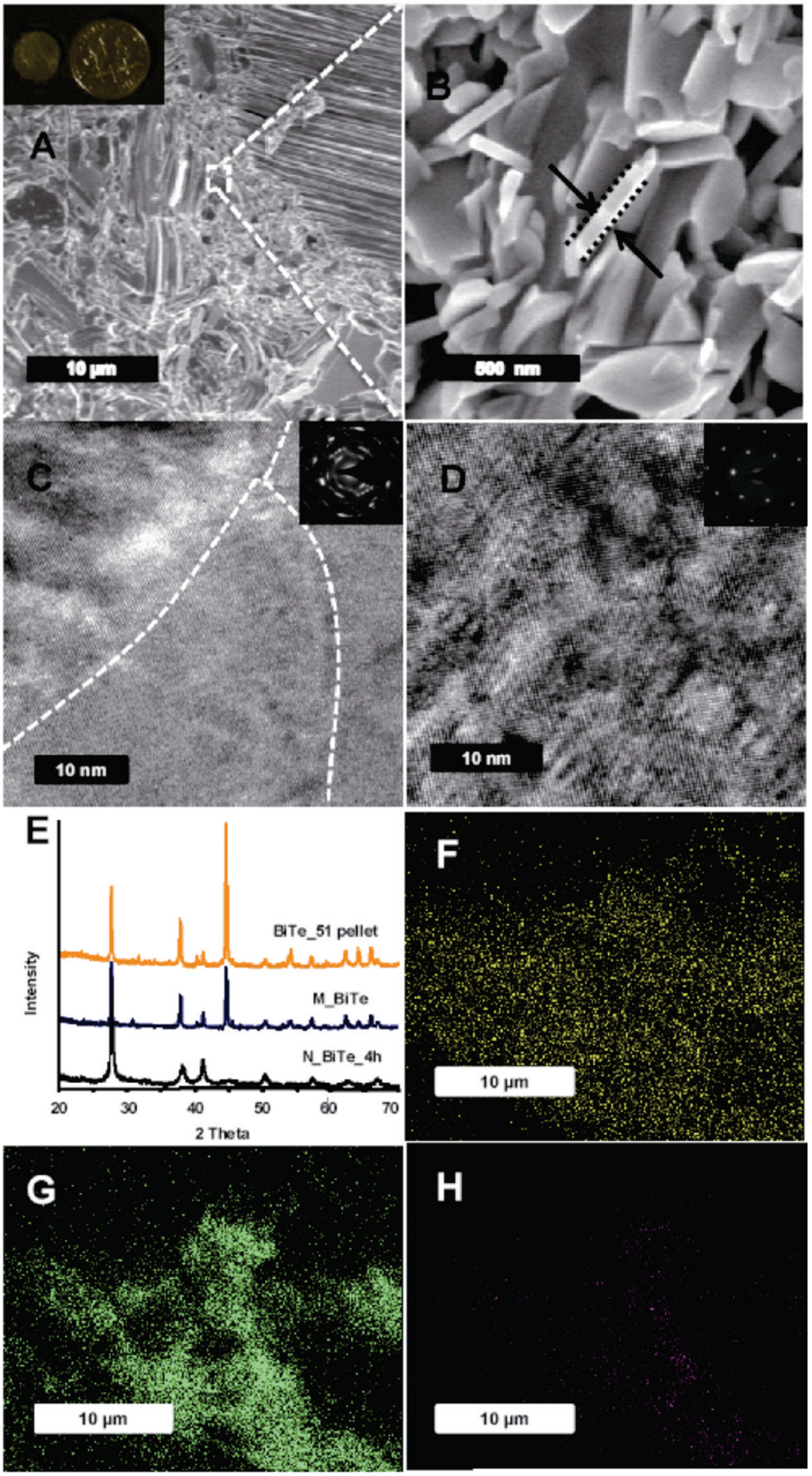

Figure 2. (A) Typical SEM image of the cross section of hot-pressed BiTe_51 pellet; the inset is the optical image of as-prepared BiTe_51 pellet. (B) Zoom-in on selected area in (A). (C) HR-TEM image of one lamellar of BiTe_51; the dashed line shows the grain boundaries, and the inset is the corresponding SAED that indicates its polycrystalline structure. (D) HR-TEM image of a single grain of BiTe_51, and the inset is the corresponding SAED pattern; the direction of view is [0001]. (E) XRD patterns of BiTe_51, M_BiTe, and N_BiTe_4h. EDX element mapping of Bi (F), Te (G), and Ni (H).

The Ni nanospheres are galvanically displaced to form the Bi_2Te_3−Te polycrystalline spheres (Figure 1B and Figure S1 in Supporting Information) with an average diameter of 200 nm, close in size to the original Ni spheres. The Kirkendall effect is not significant. The main reason for this is that, in our replacement synthesis, the preformed Ni nanospheres are not homogeneously dispersed by surfactants; during the synthesis, they aggregate to a certain extent to give a chaotic diffusion of Ni atoms. With longer ultrasonication time, porous Bi_2Te_3−Te spheres are observed as shown in Figure S2. Accordingly, only ∼1 min of ultrasonication is applied to promote dispersion and ensure that the compressed ingot had mechanic and transport properties suitable for thermoelectric material.

X-ray diffraction confirmed the presence of Bi_2Te_3 (Figure S3A in Supporting Information). Rietveld refinement (Figure S3C) suggests that the material contains amorphous Te and residual (<3 wt %) $NiTe_2$ in addition to the major Bi_2Te_3 phase. The average grain size (∼25 nm) calculated from the Scherrer equation is consistent with the crystal domain sizes observed by high-resolution TEM (HR-TEM) (Figure S1). The stoichiometry of the replaced products was determined by inductively coupled plasma (ICP) spectrometric analysis (Figure S3B), which showed all samples to be rich in tellurium independent of the reaction time, as was also previously observed by others.[31] A lower Te/Bi ratio (∼2/1) could be achieved by partially washing excess tellurium in 1 M aqueous NaOH. Te/Bi ratios below 2/1 were difficult to achieve because amorphous $NiTe_2$ is also produced under these reaction conditions as a side reaction. ICP results show that the product of a 4 h reaction, denoted by N_BiTe_4h, gives the lowest Ni content (<3 wt %) (Figure S3B).

After washing with 1 M NaOH for several hours, N_BiTe_4h was mixed with microscale bismuth telluride powders (M_BiTe) in various ratios. The hot-pressed ingots are denoted by BiTe_bare (only microscale particles), BiTe_101 (micro/nano = 10:1), and BiTe_51 (micro/nano = 5:1). As a reference, BiTe_21 (micro/nano = 2:1) was also prepared. Density measurements show an average relative density of ∼93% for all pressed pellets except BiTe_21 (∼80%).

The micro−nano heterostructure has several advantages for thermoelectric applications over bare bulk and bare nanocomposite materials. Nanoscale structures in the condensed pellets are crucial to reducing the thermal conductivity by introducing phonon scattering centers. The size distribution of the particle mixture is very broad, with particle diameters ranging from 100 nm to 10 μm. This permits the smallest particles to fill the voids among the largest particles, thereby improving the packing density on annealing. As a result, high-density pellets were obtained under milder hot-pressing conditions (lower pressure and lower temperature) than those reported previously.[32−34] This was found to be the case even though the nanoparticle morphology changes from spheres to plates under vacuum during the hot-pressing. Figure 2A,B shows the cross section images of a condensed pellet. The textures are formed from microscale particles with some local areas rich in nanoplates. During hot-pressing, the nanospheres recrystallize faster along the direction perpendicular to [0001] than the direction parallel to [0001]. The total volume of the nanoplate (500 nm diameter × 50 nm thickness) is approximately equivalent to that of the preformed nanospheres (250 nm diameter), suggesting that each plate is produced by compressing single preformed nanospheres. Although the morphology changes after hot-pressing, the nanocrystalline grain size is still on the nanoscale and below 50 nm. This micro/nano mixed structure was also verified by high-resolution TEM. Two thinned lamellae shown in Figure S4 are taken from the same ingot (BiTe_51). One lamella shows an oriented polycrystalline phase with grain boundaries of nanometer-sized particles. The other lamella is a micrometer-sized single crystal (Figure 2C,D). The boundaries generated by these nanoplates will scatter the phonons more efficiently in the "nano-rich area" than the "micro-rich area", leading to a lower thermal conductivity than a pellet that contains only microparticles.

Another advantage of this heterostructure synthesis approach is that it produces a material with substructures on two scales: microscale bismuth telluride powders, which generate a bulk matrix with low resistivity, and heterostructure particulate inclusions on the nanoscale, which scatter phonons.[6] Li and co-workers reported that when high-energy ball milling is used, optimal electrical properties are obtained when the ratio of fine to coarse particles is 6/4 (60 wt % fine powders).[35] In contrast, we observe enhanced electrical conductivity when the nano/micro ratio is below 1/5 (17 wt % NPs). We attribute this smaller ratio to the Bi_2Te_3−Te heterophase and the presence of residual Ni.

Figure 2E shows the X-ray diffraction patterns of the micro−nano pellet (BiTe_51) and its two components (N_BiTe_4h and M_BiTe). After hot-pressing, due to the preferred orientation, the relative counts of peaks are different from the starting materials. Also, BiTe_51 shows a minor phase of $NiTe_2$, which is generated from the amorphous Ni residue and excess Te species of N_BiTe_4h. An enlarged diffraction pattern is shown in Supporting Information Figure S5. This is consistent with a previous study on Ni/Bi_2Te_3 which reported that the reaction with Ni and Te can produce nickel telluride as a stable interphase between Ni and Bi_2Te_3.[36] EDX mappings of elements Bi, Te, and Ni (Figure 2F−H) show that neither Te nor Ni is dispersed as homogeneously as is Bi. On comparing the EDX maps with the SEM image of the same area, we find that the high

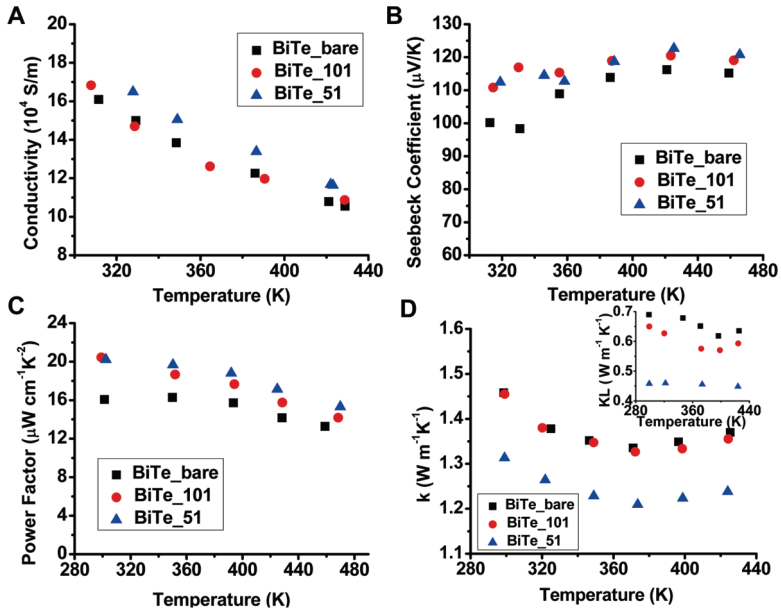

Figure 3. Temperature dependence of (A) electrical conductivity σ, (B) absolute value of Seebeck coefficient S, (C) power factor $S^2\sigma$, and (D) thermal conductivity κ of BiTe_bare, BiTe_101, and BiTe_51. The inset of (D) is the lattice part (κ_L) of thermal conductivity.

tellurium and nickel regions correspond to the nano-rich areas (Figure S6). In general, Ni is considered to be a good contact metal with a smaller atomic diffusion path length than other metals such as Sn and Cu; however, a recent study by Ren and co-workers indicates that Ni is not inert. The easy diffusion of Ni into n-type Bi_2Te_3 makes it possible to generate nickel telluride, which affects charge transport as an electron donor.[37] A more detailed analysis of the role of Ni in our materials is discussed below.

A third advantage, the absence of surfactants in our synthesis, leads to a functionalized inorganic TE material with similar behavior to that of traditional TE materials prepared by zone-melting.

The thermoelectric properties of these micro−nano heterostructures were investigated as a function of temperature from ~300 to >400 K. In contrast to other solution-grown thermoelectric NPs, the NPs prepared in this work do not require any surfactants to confine the size, which facilitates the electrical conductivity necessary for high power factor ($S^2\sigma$), as shown in Figure 3C.[16,18,19] More specifically, the absolute values of the Seebeck coefficients as well as the electrical conductivities of BiTe_101 (NP percentage 9.1%) and BiTe_51 (NP percentage 16.7%) are even slightly higher than those of BiTe_bare (NP percentage 0%). This enhancement is considered to be mainly due to the Bi_2Te_3−Te heterophase rather than the effects of the presence of $NiTe_2$ since, as an electron donor analogous to Cu and Sn in Bi_2Te_3,[38] $NiTe_2$ would be expected to have a negative effect on the power factor by substantially reducing the Seebeck coefficient. Our results show that the enhancement of the power factor by the heterophase could compensate for the negative effect of the Ni impurity when the heterophase percentage is below 20%, as shown in Figure 3C for BiTe_101 and BiTe_51. A greater fraction of nanoscaled heterophase leads to progressively more heavily Ni-doped bismuth telluride and increases the carrier concentration above the optimum range (10^{19}−10^{20} cm^{-3}). For example, the power factor of BiTe_21 is reduced to only one-third of that of BiTe_bare, as shown in Figure S7. We therefore focused on the samples with <20% Bi_2Te_3−Te heterostructures such as samples BiTe_101 and BiTe_51, which produce good results not only because of their high density but also because, at their low levels of Ni dopant (<0.5 wt %), one achieves suitable carrier concentrations (Figure S8). A more detailed study of the effect of Ni on the TE properties is in progress.

Table 1 summarizes the electrical properties of the samples described here at room temperature and compares them with published results of solution-grown bismuth (antimony) telluride.[7,16−18] For the bismuth telluride binary system, the power factor reported here is highest (zT = ~0.4 at room temperature) close to the typical figures of merit (zT = ~0.6 at room temperature) obtained from materials prepared using a high-temperature (~700 °C) melting synthesis.

In addition to a high power factor, a lower thermal conductivity (κ) is critical for good TE performance. The thermal conductivity is calculated using eq 2, in which D_t is the diffusivity, ρ is the density, and C_p is the heat capacity.

$$\kappa = D_t \times \rho \times C_p \quad (2)$$

Figure 3D shows the thermal conductivities and the lattice contributions of all samples. When more

TABLE 1. Comparison of TE Parameters of Selected Bi_2Te_3 Samples (All Values Were Recorded at Room Temperature)

sample name	Seebeck coefficient (μV/K)	electrical conductivity (10^4 S/m)	power factor (μW/(cm·K^2))	zT	reference
BiTe_bare	−100	16.5	16.1	0.30	this work
BiTe_101	−109	16.8	20.4	0.36	this work
BiTe_51	−106	17.9	20.2	0.42	this work
Bi_2Te_3	−91	0.50	0.41	0.03	16
Bi_2Te_3	−80	7.7	4.9	0.20	17
$Bi_{0.5}Sb_{1.5}Te_3$	+157	2.7	6.6	0.50	18
$Bi_{0.5}Sb_{1.5}Te_3$[a]	+187	12.5	43.7	1.20	7

[a] This is the bulk bismuth antimony telluride record reported by using zone-melting plus ball milling strategy.

nanometer-sized particles are incorporated, a lower κ is observed, mainly as a result of the lattice thermal conductivity. The lattice contribution was calculated based on the modified Wiedemann−Franz law after considering the anisotropic properties (Supporting Information). The nanoscale−particle boundaries enhance the phonon scattering and lead to a decrease of $\kappa_{\perp\perp}$ to ∼0.5 Wm^{-1} K^{-1}. These results indicate that our micro−nano heterostructured material approach leads to an improved ECPG and is thus promising as a strategy for further studies to improve TE performance of TE materials.

On the basis of both charge and phonon transport, BiTe_51 has an experimental figure of merit ∼0.5 at room temperature and ∼0.65 at 400 K. Note that these zT values are calculated on the basis of in-plane electronic conductivity and cross-plane thermal conductivity. Considering the anisotropic properties, the estimated figures of merit are calculated with a modified factor of ∼0.8 based on Yan *et al.*'s work.[39] The results are summarized in Table 1 and Supporting Information Figure S9. BiTe_51 shows an estimated figure of merit of ∼0.42 at room temperature and ∼0.55 at 400 K. Compared to our lab-made microscale material without any heterostructured NPs, BiTe_bare, this is about a 40% enhancement. A detailed study of the anisotropic TE properties of our samples will be discussed in future work.

CONCLUSION

In summary, we report a surfactant-free synthesis strategy using galvanic replacement to grow nonstoichiometric Bi_2Te_3−Te nanoparticles at low temperature and in large quantity. The heterostructured material is achieved by simply mixing "as-prepared" particles as a heterophase into commercially available (microscale) powders, then hot-pressing. The existence of the nanoscale and nonstoichiometric heterophase results in an inhomogeneous heterostructure with a figure of merit of ∼0.42 at room temperature and ∼0.55 at 400 K. Compared to this lab's bulk bismuth telluride, this heterostructured material shows a 40% enhancement in zT. This enhancement is mainly due to a decreased thermal conductivity with maintenance of the power factor. The lower thermal conductivity that is observed is attributed to the scattering of phonons by the heterostructure-generated nanoscale grain boundaries. In addition, we believe that the introduced heterophase as well as the absence of organic residue from surfactant facilitates charge transport. Due to the unique structure and promising properties, this approach indicates the potential for further improvement and large-scale thermoelectric applications. In the future, we plan to investigate a ternary system, antimony-doped bismuth telluride.

METHODS

All reagents were used directly from commercial suppliers without any purification except micro-sized Bi_2Te_3. Micro-sized Bi_2Te_3 powders were purchased from Alfa Aesar (vacuum deposition grade, 99.999%) and ground into fine powders denoted by M_BiTe.

Synthesis of Nickel Nanospheres as Starting Template and Reducing Agent. The synthesis procedure is similar to one previously reported.[40] $NiCl_2·6H_2O$ (chemical pure, ≥98%, Sigma-Aldrich) and 80% $N_2H_4·H_2O$ solution and 50 wt % NaOH aqueous solution were used as reagents. In a typical synthesis, 6.4258 g of $NiCl_2·6H_2O$ was dissolved in 7.5 mL of DI water. Under vigorous stirring, 5.48 mL of 80% $N_2H_4·H_2O$ solution was added into the solution and a pale violet precipitate could be observed. Then the solution was heated to about 65 °C. (Please note that, due to the exothermic formation of $[Ni(N_2H_4)_2]^{2+}$ complex, the hot plate was set at 60 °C.) When the temperature was above 65 °C, the hot plate was turned off in order to let it cool. When the temperature of solution decreased to 50 °C by cooling in an ambient atmosphere, 23.04 g of 50 wt % NaOH solution was poured instantaneously into the stock solution. The molar ratio of $NiCl_2/N_2H_4$/NaOH is 1.35/4.5/3.6. After 2 h reaction, the black nickel precipitate was washed several times with DI water and ethanol. The crude product was dried in a vacuum oven (60 °C) overnight and stored in vacuum. The total yield of this reaction is close to 100%.

Synthesis of Bismuth Telluride by Galvanic Replacement. Under ultrasonication, 1 g of as-prepared Ni nanospheres was added into 630 mL of 0.006 M Bi^{3+}/0.009 M $HTeO_2^+$ precursor (pH = 1). The mixture was mechanically stirred vigorously for 3 (N_BiTe_3h), 4 (N_BiTe_4h), and 6 h (N_BiTe_6h), and the black precipitates were collected after filtration. The products were washed by 1 M NaOH solution, then vacuum-dried overnight.

Fabrication of Condensed Micro−Nano Mixed Pellet by Hot-Pressing. N_BiTe_4h and M_BiTe were mixed in different ratios (1:10, 1:5, and 1:2) and hot-pressed into a pellet under 140 psi at 350 °C. The pellet after hot-pressing was roughly polished by 400 and 600 grit sandpaper. The prepared pellets were denoted by

BiTe_101, BiTe_51, and BiTe_21, respectively. Bare M_BiTe powder was hot-pressed under the same conditions into BiTe_-bare pellet as a reference.

Materials Characterizations. Wide-angle XRD (WAXRD) data were obtained on a Bruker D8 diffractometer with Cu Kα radiation, and Rietveld-refined using ReX software (http://www.rexpd.com/rex/). Transmission electron microscopy (TEM) images were taken using a FEI T20 electron microscope operating at 200 keV. Specimens suitable for high-resolution electron microscopy observations were prepared by low-angle ion milling to electron transparency (~70 nm) through a FEI DB235 dual-beam FIB system. High-resolution TEM images were taken using FEI Titan TEM/STEM. Scanning electron microscopy (SEM) images and energy-dispersive using X-ray analysis (EDX) were taken on a Philips XL40 electron microscope. The element analysis was done by an inductively coupled plasma (ICP) spectrometer on Thermo iCAP 6300.

Thermoelectric Properties Measurements. Low-temperature transport properties were characterized from room temperature to 150 °C under dynamic vacuum at the Caltech thermoelectrics laboratory. Electrical resistivity was determined using the van der Pauw technique, and the Hall coefficient was measured with a 2 T field and pressure-assisted contacts. The Seebeck coefficient was measured using Chromel-Nb thermocouples and by allowing the temperature gradient across the sample to oscillate between ±10 K. A Netzsch LFA 457 was used to measure the thermal diffusivity. The heat capacity was estimated using the Dulong−Petit value.

Acknowledgment. The authors sincerely thank A. Palmqvist, C. Levi, G. Zeng, R. Leckie, D. Cederkrantz, K. Fields, B. Curtin, and A. Ivanovskaya for helpful discussions and assistance with instrument use. This work was supported in part by the Center for Energy Efficient Materials (CEEM), an Energy Frontier Research Center funded by the U.S. Department of Energy, Office of Basic Energy Sciences under Award Number DE-SC0001009, and in part by the National Science Foundation under Grant No. DMR-0805148. The MRL Central Facilities are supported by the MRSEC Program of the NSF under Award No. DMR05-20415, a member of the NSF-funded Materials Research Facilities Network (www.mrfn.org).

Supporting Information Available: Calculation of lattice contribution in thermal conductivity. SEM images of the selected cross area for EDX mapping. TEM images of as-prepared porous bismuth telluride nanoparticles and the thinned lamellas for HR-TEM. XRD patterns and the Rietveld refinement result of the products after reacting. Enlarged XRD pattern of BiTe_51 in Figure 4C. ICP results of Te/Bi stoichiometry and Ni contents of as-prepared powders. The temperature dependence of the electrical properties of BiTe_21. The mobility, concentration, and estimated figures of merit (*zT* values) of all materials as a function of temperature. This material is available free of charge *via* the Internet at http://pubs.acs.org.

REFERENCES AND NOTES

1. Boukai, A. I.; Bunimovich, Y.; Tahir-Kheli, J.; Yu, J.-K.; Goddard, W. A., III; Heath, J. R. Silicon Nanowires as Efficient Thermoelectric Materials. *Nature* **2008,** *451*, 168–171.
2. Dresselhaus, M.; Chen, G.; Tang, M.; Yang, R.; Lee, H.; Wang, D.; Ren, Z.; Fleurial, J. P.; Gogna, P. New Directions for Low-Dimensional Thermoelectric Materials. *Adv. Mater.* **2007,** *19*, 1043–1053.
3. Dresselhaus, M. S.; Chen, G.; Ren, Z.; Fleurial, J.-P.; Gogna, P.; Tang, M. Y.; Vashaee, D.; Lee, H.; Wang, X.; Joshi, G.; Zhu, G.; Wang, D.; Blair, R.; Bux, S.; Kaner, R. Nanocomposites to Enhance ZT in Thermoelectrics. *Mater. Res. Soc. Symp. Proc.* **2008,** *1044*, U02–04.
4. Hochbaum, A. I.; Chen, R.; Delgado, R. D.; Liang, W.; Garnett, E. C.; Najarian, M.; Majumdar, A.; Yang, P. Enhanced Thermoelectric Performance of Rough Silicon Nanowires. *Nature* **2008,** *451*, 163–167.
5. Kanatzidis, M. G. Nanostructured Thermoelectrics: The New Paradigm?. *Chem. Mater.* **2010,** *22*, 648–659.
6. Kim, W.; Zide, J.; Gossard, A.; Klenov, D.; Stemmer, S.; Shakouri, A.; Majumdar, A. Thermal Conductivity Reduction and Thermoelectric Figure of Merit Increase by Embedding Nanoparticles in Crystalline Semiconductors. *Phys. Rev. Lett.* **2006,** *96*, 045901.
7. Poudel, B.; Hao, Q.; Ma, Y.; Lan, Y.; Minnich, A.; Yu, B.; Yan, X.; Wang, D.; Muto, A.; Vashaee, D.; Chen, X.; Liu, J.; Dresselhaus, M. S.; Chen, G.; Ren, Z. High-Thermoelectric Performance of Nanostructured Bismuth Antimony Telluride Bulk Alloys. *Science* **2008,** *320*, 634–638.
8. Lan, Y.; Minnich, A. J.; Chen, G.; Ren, Z. Enhancement of Thermoelectric Figure-of-Merit by a Bulk Nanostructuring Approach. *Adv. Funct. Mater.* **2010,** *20*, 357–376.
9. Saramat, A.; Svensson, G.; Palmqvist, A. E. C.; Stiewe, C.; Mueller, E.; Platzek, D.; Williams, S. G. K.; Rowe, D. M.; Bryan, J. D.; Stucky, G. D. Large Thermoelectric Figure of Merit at High Temperature in Czochralski-Grown Clathrate $Ba_8Ga_{16}Ge_{30}$. *J. Appl. Phys.* **2006,** *99*, 023708.
10. Snyder, G. J.; Toberer, E. S. Complex Thermoelectric Materials. *Nat. Mater.* **2008,** *7*, 105–114.
11. Sootsman, J. R.; Chung, D. Y.; Kanatzidis, M. G. New and Old Concepts in Thermoelectric Materials. *Angew. Chem., Int. Ed.* **2009,** *48*, 8616–8639.
12. Vineis, C. J.; Shakouri, A.; Majumdar, A.; Kanatzidis, M. G. Nanostructured Thermoelectrics: Big Efficiency Gains from Small Features. *Adv. Mater.* **2010,** *22*, 3970–3980.
13. Ahn, K.; Han, M.-K.; He, J.; Androulakis, J.; Ballikaya, S.; Uher, C.; Dravid, V. P.; Kanatzidis, M. G. Exploring Resonance Levels and Nanostructuring in the PbTe−CdTe System and Enhancement of the Thermoelectric Figure of Merit. *J. Am. Chem. Soc.* **2010,** *132*, 5227–5235.
14. Vashaee, D.; Shakouri, A. Improved Thermoelectric Power Factor in Metal-Based Superlattices. *Phys. Rev. Lett.* **2004,** *92*, 106103.
15. Zhao, X. B.; Ji, X. H.; Zhang, Y. H.; Zhu, T. J.; Tu, J. P.; Zhang, X. B. Bismuth Telluride Nanotubes and the Effects on the Thermoelectric Properties of Nanotube-Containing Nanocomposites. *Appl. Phys. Lett.* **2005,** *86*, 062111.
16. Dirmyer, M. R.; Martin, J.; Nolas, G. S.; Sen, A.; Badding, J. V. Thermal and Electrical Conductivity of Size-Tuned Bismuth Telluride Nanoparticles. *Small* **2009,** *5*, 933–937.
17. Scheele, M.; Oeschler, N.; Meier, K.; Kornowski, A.; Klinke, C.; Weller, H. Synthesis and Thermoelectric Characterization of Bi_2Te_3 Nanoparticles. *Adv. Funct. Mater.* **2009,** *19*, 3476–3483.
18. Scheele, M.; Oeschler, N.; Veremchuk, I.; Reinsberg, K.-G.; Kreuziger, A.-M.; Kornowski, A.; Broekaert, J.; Klinke, C.; Weller, H. ZT Enhancement in Solution-Grown $Sb_{(2-x-)Bix}Te_3$ Nanoplatelets. *ACS Nano* **2010,** *4*, 4283–4291.
19. Mehta, R. J.; Karthik, C.; Singh, B.; Teki, R.; Borca-Tasciuc, T.; Ramanath, G. Seebeck Tuning in Chalcogenide Nanoplate Assemblies by Nanoscale Heterostructuring. *ACS Nano* **2010,** *4*, 5055–5060.
20. Datta, A.; Paul, J.; Kar, A.; Patra, A.; Sun, Z.; Chen, L.; Martin, J.; Nolas, G. S. Facile Chemical Synthesis of Nanocrystalline Thermoelectric Alloys Based on Bi-Sb-Te-Se. *Cryst. Growth Des.* **2010,** *10*, 3983–3989.
21. Mi, J.-L.; Lock, N.; Sun, T.; Christensen, M.; Sondergaard, M.; Hald, P.; Hng, H. H.; Ma, J.; Iversen, B. B. Biomolecule-Assisted Hydrothermal Synthesis and Self-Assembly of Bi_2Te_3 Nanostring-Cluster Hierarchical Structure. *ACS Nano* **2010,** *4*, 2523–2530.
22. Kovalenko, M. V.; Spokoyny, B.; Lee, J.-S.; Scheele, M.; Weber, A.; Perera, S.; Landry, D.; Talapin, D. V. Semiconductor Nanocrystals Functionalized with Antimony Telluride Zintl Ions for Nanostructured Thermoelectrics. *J. Am. Chem. Soc.* **2010,** *132*, 6686–6695.
23. Skrabalak, S. E.; Chen, J.; Sun, Y.; Lu, X.; Au, L.; Cobley, C. M.; Xia, Y. Gold Nanocages: Synthesis, Properties, and Applications. *Acc. Chem. Res.* **2008,** *41*, 1587–1595.
24. Sun, Y.; Wiley, B.; Li, Z.-Y.; Xia, Y. Synthesis and Optical Properties of Nanorattles and Multiple-Walled Nanoshells/Nanotubes Made of Metal Alloys. *J. Am. Chem. Soc.* **2004,** *126*, 9399–9406.

25. Vasquez, Y.; Henkes, A. E.; Chris Bauer, J.; Schaak, R. E. Nanocrystal Conversion Chemistry: A Unified and Materials-General Strategy for the Template-Based Synthesis of Nanocrystalline Solids. *J. Solid State Chem.* **2008,** *181*, 1509–1523.
26. Hangarter, C. M.; Lee, Y. I.; Hernandez, S. C.; Choa, Y. H.; Myung, N. V. Nanopeapods by Galvanic Displacement Reaction. *Angew. Chem., Int. Ed.* **2010,** *49*, 7081–7085.
27. Xiao, F.; Yoo, B.; Lee, K. H.; Myung, N. V. Synthesis of Bi_2Te_3 Nanotubes by Galvanic Displacement. *J. Am. Chem. Soc.* **2007,** *129*, 10068–10069.
28. Moon, G. D.; Ko, S.; Xia, Y.; Jeong, U. Chemical Transformations in Ultrathin Chalcogenide Nanowires. *ACS Nano* **2010,** *4*, 2307–2319.
29. Martin-Gonzalez, M. S.; Prieto, A. L.; Gronsky, R.; Sands, T.; Stacy, A. M. Insights into the Electrodeposition of Bi_2Te_3. *J. Electrochem. Soc.* **2002,** *149*, C546–C554.
30. Gupta, R. P.; Xiong, K.; White, J. B.; Cho, K.; Alshareef, H. N.; Gnade, B. E. Low Resistance Ohmic Contacts to Bi_2Te_3 Using Ni and Co Metallization. *J. Electrochem. Soc.* **2010,** *157*, H666–H670.
31. Jung, H.; Rheem, Y.; Chartuprayoon, N.; Lim, J. H.; Lee, K. H.; Yoo, B.; Lee, K. J.; Choa, Y. H.; Wei, P.; Shi, J.; Myung, N. V. Ultra-long Bismuth Telluride Nanoribbons Synthesis by Lithographically Patterned Galvanic Displacement. *J. Mater. Chem.* **2010,** *20*, 9982–9987.
32. Girard, S. N.; He, J.; Li, C.; Moses, S.; Wang, G.; Uher, C.; Dravid, V. P.; Kanatzidis, M. G. *In Situ* Nanostructure Generation and Evolution within a Bulk Thermoelectric Material To Reduce Lattice Thermal Conductivity. *Nano Lett.* **2010,** *10*, 2825–2831.
33. Ma, Y.; Hao, Q.; Poudel, B.; Lan, Y.; Yu, B.; Wang, D.; Chen, G.; Ren, Z. Enhanced Thermoelectric Figure-of-Merit in p-Type Nanostructured Bismuth Antimony Tellurium Alloys Made from Elemental Chunks. *Nano Lett.* **2008,** *8*, 2580–2584.
34. Xie, W.; He, J.; Kang, H. J.; Tang, X.; Zhu, S.; Laver, M.; Wang, S.; Copley, J. R. D.; Brown, C. M.; Zhang, Q.; Tritt, T. M. Identifying the Specific Nanostructures Responsible for the High Thermoelectric Performance of $(Bi,Sb)_2Te_3$ Nanocomposites. *Nano Lett.* **2010,** *10*, 3283–3289.
35. Zhao, L.-D.; Zhang, B.-P.; Liu, W.-S.; Li, J.-F. Effect of Mixed Grain Sizes on Thermoelectric Performance of Bi_2Te_3 Compound. *J. Appl. Phys.* **2009,** *105*, 023704.
36. Xiong, K.; Lee, G.; Gupta, R. P.; Wang, W.; Gnade, B. E.; Cho, K. Behaviour of Group IIIA Impurities in PbTe: Implications To Improve Thermoelectric Efficiency. *J. Phys. D: Appl. Phys.* **2010,** *43*, 405403.
37. Lan, Y. C.; Wang, D. Z.; Chen, G.; Ren, Z. F. Diffusion of Nickel and Tin in p-Type $(Bi,Sb)_2Te_3$ and n-Type $Bi_2(Te,Se)_3$ Thermoelectric Materials. *Appl. Phys. Lett.* **2008,** *92*, 101910.
38. Svechnikova, T.; Nikhezina, I.; Polikarpova, N. Properties of Bi_2Te_3 Single Crystals Doped with Sn. *Inorg. Mater.* **2000,** *36*, 765–767.
39. Yan, X.; Poudel, B.; Ma, Y.; Liu, W. S.; Joshi, G.; Wang, H.; Lan, Y.; Wang, D.; Chen, G.; Ren, Z. F. Experimental Studies on Anisotropic Thermoelectric Properties and Structures of n-Type $Bi_2Te_{2.7}Se_{0.3}$. *Nano Lett.* **2010,** *10*, 3373–3378.
40. Choi, J. Y.; Lee, Y. K.; Yoon, S. M.; Lee, H. C.; Kim, B. K.; Kim, J. M.; Kim, K. M.; Lee, J. H. A Chemical Route to Large-Scale Preparation of Spherical and Monodisperse Ni Powders. *J. Am. Ceram. Soc.* **2005,** *88*, 3020–3023.